

Solute segregation in polycrystalline aluminum from hybrid Monte Carlo and molecular dynamics simulations with a unified neuroevolution potential

Keke Song,^{1,2} Jiahui Liu,^{1,3} Shunda Chen,^{4, a)} Zheyong Fan,^{5, b)} Yanjing Su,^{1,3, c)} and Ping Qian^{1,2, d)}

¹⁾Beijing Advanced Innovation Center for Materials Genome Engineering,
University of Science and Technology Beijing, Beijing 100083, China

²⁾Department of Physics, University of Science and Technology Beijing, Beijing 100083,
China

³⁾Corrosion and Protection Center, University of Science and Technology Beijing, Beijing 100083,
China

⁴⁾Department of Civil and Environmental Engineering, George Washington University, Washington,
DC 20052, USA

⁵⁾College of Physical Science and Technology, Bohai University, Jinzhou,
P. R. China

(Dated: 23 April 2024)

One of the most effective methods to enhance the strength of aluminum alloys involves modifying grain boundaries (GBs) through solute segregation. However, the fundamental mechanisms of solute segregation and their impacts on material properties remain elusive. In this study, we implemented highly efficient hybrid Monte Carlo and molecular dynamics (MCMD) algorithms in the graphics process units molecular dynamics (GPUMD) package. Using this efficient MCMD approach combined with a general-purpose machine-learning-based neuroevolution potential (NEP) for 16 elemental metals and their alloys, we simulated the segregation of 15 solutes in polycrystalline Al. Our results elucidate the segregation behavior and trends of 15 solutes in polycrystalline Al. Additionally, we investigated the impact of solutes on the strength of polycrystalline Al. The mechanisms underlying solute strengthening and embrittlement were analyzed at the atomistic level, revealing the importance of GB cohesion, as well as the nucleation and movement of Shockley dislocations, in determining the material's strength. We anticipate that our developed methods, along with our insights into solute segregation behavior in polycrystalline Al, will be valuable for the design of Al alloys and other multi-component materials, including medium-entropy materials, high-entropy materials, and complex concentrated alloys.

I. INTRODUCTION

Aluminum alloys are widely recognized for their versatility in various structural applications due to their lightweight nature (low density), high strength, and good corrosion resistance^{1,2}. Comprehensively understanding and enhancing the structural properties of aluminum alloys is crucial for unlocking their vast potential in engineering applications. Grain boundaries (GBs) are prevalent defects in metallic alloys that govern the macroscopic strength of materials³⁻⁵. Solute segregation at GBs profoundly impacts the structure, composition, and overall properties of alloys, offering a promising avenue for developing materials with enhanced performance⁶⁻⁸. Despite considerable research on the effects of solute segregation on GBs stability and strengthening⁹⁻¹⁵, fundamental questions regarding the mechanisms and impacts of solute segregation on material properties persist, primarily due to the challenges associated with observing segregation at the atomic level in situ.

Atomistic simulation methods, particularly *ab ini-*

tio calculations based on quantum-mechanical density-functional theory (DFT), have emerged as valuable tools for understanding solute segregation behavior at GBs. For instance, Wu *et al.* investigated the strengthening effect of transition metals on a series of tungsten GBs, revealing insights into their dependence on GB structure and solute radius¹¹. Additionally, Mahjoub *et al.* conducted extensive DFT calculations to reveal the general trend of segregation at GBs for a large number of solutes in the periodic table¹⁰. Recently, Song *et al.* studied the effects of the concentration of alloying elements in Fe GBs on their strength, hydrogen atom trapping, and hydrogen-induced embrittlement¹⁶.

However, DFT calculations are constrained by efficiency limitations, restricting the analysis of solute atom segregation to specific GBs while largely ignoring temperature effects. In contrast, molecular dynamics (MD) simulations with classical potentials allow for the exploration of larger structures while considering temperature effects, providing valuable insights into realistic physical process¹⁷⁻²⁰. Most previous works have used the embedded-atom method (EAM) potential or its extensions^{21,22}, which often lack the desired accuracy, particularly for alloys.

In this paper, we utilize the highly accurate and efficient machine learning potential, UNEP-v1, recently developed by Song *et al.*²³ as a general-purpose unified neu-

^{a)}Electronic mail: phychensd@gmail.com

^{b)}Electronic mail: brucenju@gmail.com

^{c)}Electronic mail: yjsu@ustb.edu.cn

^{d)}Electronic mail: qianping@ustb.edu.cn

roevolution potential (NEP)^{24–26}, for 16 elemental metals and their alloys (Ag, Al, Au, Cr, Cu, Mg, Mo, Ni, Pb, Pd, Pt, Ta, Ti, V, W, Zr), to investigate solute segregation in polycrystalline Al. It has been shown that UNEP-v1 outperforms the EAM potential by Zhou *et al.*²⁷ for various physical properties²³. To facilitate our investigation, we develop an efficient implementation of the hybrid Monte Carlo and molecular dynamics (MCMD) method closely integrated with the NEP model in the GPUMD package²⁸. Employing this method, we systematically study the distribution of 15 solutes in polycrystalline Al. Our analysis reveals that Ag, Au, Cu, Mg, Pb, Pd, and Pt in polycrystalline Al tend to fully segregate at GBs, while Ni, and Zr exhibit partially segregation at GBs. Additionally, we observe that Cr, Mo, V, W, and Ti do not segregate at GBs, with Ti precipitated as BCC TiAl within crystal lattice. Subsequently, we investigate the impact of solute segregation on the strength of polycrystalline Al. Our findings indicate that Pd and Pt significantly enhance the strength of polycrystalline Al. Furthermore, we analyze the mechanisms underlying the strengthening and embrittlement associated with solute segregation in polycrystalline Al at the atomistic level, shedding light on the crucial role of grain boundary cohesion, as well as the nucleation and movement of Shockley dislocations determining the strength of polycrystalline Al.

II. COMPUTATIONAL DETAILS AND STRUCTURAL MODELS

A. The unified neuroevolution potential for 16 elemental metals and their alloys

We employ the UNEP-v1²³ machine learning potential model based on the NEP^{24–26} approach as implemented in the GPUMD package²⁸. UNEP-v1 serves as a general-purpose potential for 16 elemental metals (Ag, Al, Au, Cr, Cu, Mg, Mo, Ni, Pb, Pd, Pt, Ta, Ti, V, W, Zr) and their alloys. As demonstrated by Song *et al.*²³, it outperforms the EAM potential by Zhou *et al.*²⁷ across various physical properties such as elastic constants, surface formation energy, vacancy formation energy, melting point, phonon dispersions, while maintaining comparable computational speed. For the first time, the UNEP-v1 machine learning potential enabled 100-million-atom atomistic simulations of alloys with *ab initio* accuracy using only eight A100 GPUs²³.

B. Building the initial polycrystalline Al model

We utilized the Voronoi algorithm as implemented in ATOMSK²⁹ to construct the initial polycrystalline Al model (Fig. 1). The model contains 6 grains in a cubic simulation cell, each side of 20 nm, totalling 490 000 atoms. To release the atomic stress in the GB regions, a series of MD simulations were conducted using GPUMD²⁸

with the UNEP-v1 machine learning potential²³. These simulations included a heating process of 200 ps from 300 to 400 K, an annealing process of 200 ps from 400 to 300 K, and finally, an equilibration process of 100 ps at 300 K. These MD simulations were performed in the NpT (constant number of atoms, pressure, and temperature) ensemble with a zero isotropic target pressure and an integration time step of 1 fs. To study solute segregation, we randomly substitute 1% Al atoms by the solute atoms, before doing the MCMD simulations as described below.

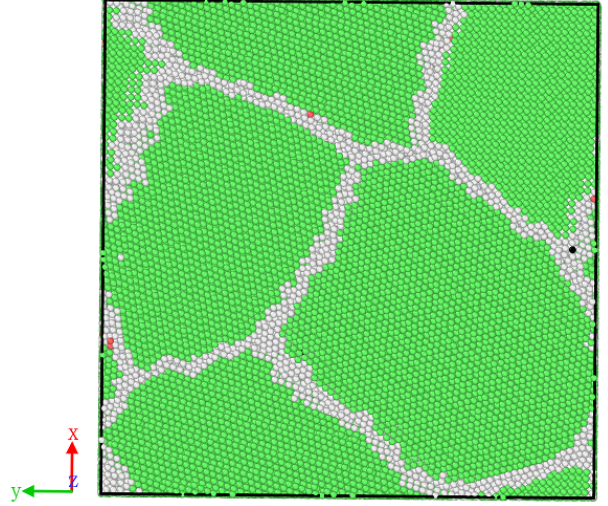


FIG. 1. Snapshot of the initial pure polycrystalline Al microstructure obtained from MD annealing simulation. Green, red, and black spheres represent atoms with local bonding features resembling FCC, HCP, and BCC (very rare) structures, respectively. Gray spheres represent atoms at the GBs.

C. An efficient MCMD approach implemented in GPUMD

MCMD proves to be an effective approach for achieving optimal chemical ordering at specific temperatures. In our study, we use the canonical MCMD (N_iVT ensemble) to investigate the segregation of solute in polycrystalline Al, where N_i is the number of atoms for species i . This canonical Monte Carlo (MC) ensemble can be realized by swapping atom pairs with different species. For each MC trial, we randomly pick two atoms of different species and swap their identities, including masses and velocities. The swap is accepted with the probability

$$P = \min \left\{ 1, \exp \left(-\frac{\Delta U}{k_B T} \right) \right\}, \quad (1)$$

where ΔU is the change in potential energy due to the trial swap. In MCMD, the MC and MD simulations are executed alternately. Specifically, we conduct 100 MC trials (regardless of acceptance) after every 100 MD steps.

For each MC trial swap, evaluating the change in potential energy, ΔU , can be achieved by at least two approaches. A straightforward approach involves recalculating the potential energy of the entire system after each attempted swap (regardless of whether the swap is accepted) and comparing it with the potential energy before the swap, which can be retrieved from the previous accepted MC trial. Usually, forces and stresses are also calculated along with energy calculation in this approach. Consequently, one MC trial in this approach nearly matches the computational cost of a MD step. With an equal ratio for MC and MD simulations, MCMD is thus twice as costly as pure MD for completing the same number of MD steps. This is the approach adopted by LAMMPS³⁰ for a general potential model.

A more efficient approach is to leverage the locality properties of the potential model and calculate site energies only for atoms that are affected by the attempted swap. In the worst-case scenario, where the two atoms to be swapped are widely separated, we still only need to calculate the site energy for about $4M$ atoms, where M is the average number of neighbors for one atom. The factor of 4 comes from the two atoms (a factor of 2) before and after the swap (another factor of 2). The computational cost for one MC trial in this approach is thus independent of the number of atoms N in the system. In this study, where $N = 490\,000$ and $M \approx 60$, the computational cost of one MC trial is only about 0.05% of that for one MD step. With an equal ratio for MC and MD simulations, this MCMD approach is nearly as fast as pure MD for completing the same number of MD steps. In other words, the MC part is *nearly free* in this approach when $N \gg M$. This is the approach we implemented in GPUMD²⁸ during the course of this study. A sample input script for performing MCMD simulation in GPUMD is provided in Appendix A.

D. Tensile loading

During dynamic tension, uniaxial tensile strain was applied at a constant strain rate of 10^8 s^{-1} by continuously scaling the atomic coordinates and box dimension along the y direction. Throughout the simulation, the NVT ensemble was simulated at 300 K with the integration time step set to 1 fs. Atomic configuration and dislocation analysis were performed using the Open Visualization Tool³¹. A sample input script for performing tensile loading simulation in GPUMD is given in Appendix B.

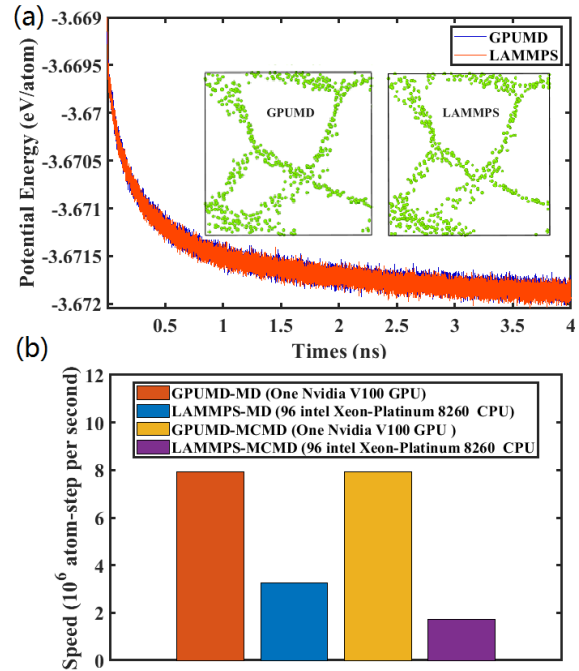


FIG. 2. (a) Potential energy versus MCMD simulation time for Mg solute segregation in polycrystalline Al, using MCMD methods implemented in GPUMD and LAMMPS. Insets illustrate the distribution of Mg atoms in the 2-nm-thick slices (xy plane, z-axis range 10 to 12 nm) extracted from the equilibrated structures obtained from MCMD simulations. (b) Computational speed comparison between GPUMD (utilizing a single Nvidia Tesla V100 GPU) and LAMMPS (utilizing 96 intel Xeon-Platinum 8260 CPUs). Note: The GPU and CPU resources mentioned above are of comparable price. The MCMD approach implemented in GPUMD demonstrates a 4x speedup compared to LAMMPS. Utilizing a single RTX4090 GPU (which is even lower in price) can further enhance the speedup to about 10x (not shown here), attributed to the efficient GPU implementation and the *nearly cost-free* MC part in the MCMD algorithm in GPUMD.

III. RESULTS AND DISCUSSION

A. Comparison of MCMD methods implemented in GPUMD and LAMMPS

Before applying the MCMD method we implemented in GPUMD²⁸ to systematically study solute segregation in polycrystalline Al, we first evaluate its performance compared to the implementation in LAMMPS³⁰, using Mg solute as an example. Both algorithms produced equivalent physical results, as evidenced by the nearly identical time evolution of the potential energy shown in Fig 2 (a). Furthermore, the configurations of Mg segregation at the GBs are also highly consistent between the two algorithms, as indicated in the insets of Fig 2 (a).

Regarding the computational efficiency (Fig 2 (b)), the NEP model as implemented in GPUMD achieves a speed

of about 7.9×10^6 atom-step/second in MD simulations using a single V100 GPU. In contrast, the NEP model as implemented in LAMMPS reaches a speed of only about 3.3×10^6 atom-step/second, using 96 Intel Xeon Platinum 8260 CPUs. When using MCMD with an equal ratio for MC and MD simulations, the GPUMD implementation achieves nearly the same speed as in pure MD simulations, while the LAMMPS implementation experiences an almost halved speed. These timings are expected according to our analyses in Sec. II C. It is noteworthy that the GPU and CPU resources mentioned above are of comparable price. The MCMD approach implemented in GPUMD demonstrates a 4x speedup compared to LAMMPS. With a single RTX4090 desktop GPU (which is even lower in price) or a single A100 GPU, the speedup is about 10x (not shown here).

B. Segregation of solute in polycrystalline Al

Using the developed MCMD algorithm in GPUMD, we systematically simulated 15 binary systems where 1% of the Al atoms in the initial polycrystalline Al structure were randomly selected and substituted by one of the following species: Ag, Au, Cr, Cu, Mg, Mo, Ni, Pb, Pd, Pt, Ta, Ti, V, W, and Zr. After 5 million MD and MC steps, the potential energies for all binary systems are well converged, and the atomic configurations can be regarded as fully equilibrated. Examination of the equilibrium configurations reveals diverse segregation behaviors for the 15 species in polycrystalline Al, which can be broadly categorized into the following four categories:

- Category 1 (7 species): Ag, Au, Cu, Mg, Pb, Pd, Pt (Figs. 3(a)-3(g)). For these species, the solute atoms all segregate to the GBs.
- Category 2 (4 species): Ni, Ta, Zr, Mo (Figs. 3(h)-3(k)). For these species, the solute atoms partially segregate to the GBs while remaining partially in the grains.
- Category 3 (3 species): Cr, V, W (Figs. 3(l)-3(n)). For these species, the solute atoms are more or less randomly distributed in the system.
- Category 4 (1 species): Ti (Fig. 3(o)). In this case, the solute atoms precipitate within the grains.

From the above four segregation behaviors, we can see that the segregation concentration of Ag, Au, Cu, Mg, Pb, Pd, and Pt solutes in polycrystalline Al is equal to or greater than the initially set 1% atomic ratio. Among them, Mg and Cu have also been experimentally³²⁻³⁵ and theoretically³⁶⁻³⁹ verified. The segregation concentration of Ni, Ta, Mo and Zr is less than the initially set concentration of 1%. The observation that Ti does not segregate at GBs aligns with DFT calculations⁴⁰. The precipitation of TiAl within the crystal is plausible, as TiAl metallic compounds are known to be stable and have been extensively studied⁴¹⁻⁴³. This is expected to influence the

properties of the Al alloy. It is noteworthy that Pb segregation in polycrystalline can cause lattice expansion by 0.4%, while other solutes affect the lattice within 0.05%. Even if all Pb atoms segregate to the GBs, the polycrystalline material will still expand, significantly affecting its strength. In the GB region, atomic arrangement differs from the bulk, resulting in the formation of loose and compressed sites due to atomic distortions. These sites offer ample opportunities for the segregation of solutes of varying sizes.

Given that our model surpasses the size calculated by DFT, the GB region provides a complex and more realistic environment that better reflects the solute segregation behavior. This aspect offers valuable insights for future simulations of solute segregation in polycrystalline Al and for the experimental design of solute segregation components in Al alloys.

C. Impact of solute segregation on the strength and deformation mechanism of polycrystalline Al

The relationship between tensile strength and strain of polycrystalline Al with various solutes is shown in Fig 4 (a). It is evident from the figure that Pt, Pd, Ta, Zr, Cr, V, Mo, Ti enhances the tensile strength of polycrystalline Al, whereas the remaining solutes reduce its strength. Strengthening solute (for Pt, Pd, and Zr) not only enhances the strength of polycrystalline Al but also enhances the maximum tensile strain. Since Ti, Cr, V, Mo, and W do not segregate at GBs, they will not be discussed further.

Fig 5 displays snapshots of pure polycrystalline Al under different deformations. Polycrystalline Al deformation goes through three stages. Initially, within the strain range of 0-4.9%, the material exhibits elastic deformation. In the strain range of 4.9-8.3%, dislocations and stacking faults are emitted from the GBs. And at 8.3% strain, cracks initiate at the GB and then propagate along the GB.

Fig 5 (a) shows the $1/6\langle 112 \rangle$ Shockley dislocations and stacking faults in pure polycrystalline Al at a strain of 4.9%. In the process of material deformation, dislocations emitted from the GBs play a decisive role⁴⁴⁻⁴⁷. Dislocation nucleation and propagation serve as the primary mechanisms for accommodating system stress. The slip and interplay of dislocations inside the grains facilitate stress redistribution throughout the plastic deformation phase.

When the strain reaches 8.3%, cracks are formed, as shown in Fig 5 (c), and the tensile stress reaches a maximum of 4.5 Gpa. In Fig 5 (b), before crack formation, no defect formation and movement is observed in the crack initiation area. This indicates weak GB cohesion, leading to intergranular cracking before the maximum stress value for defect nucleation. As strain increases, cracks propagate along the GB, ultimately resulting in material

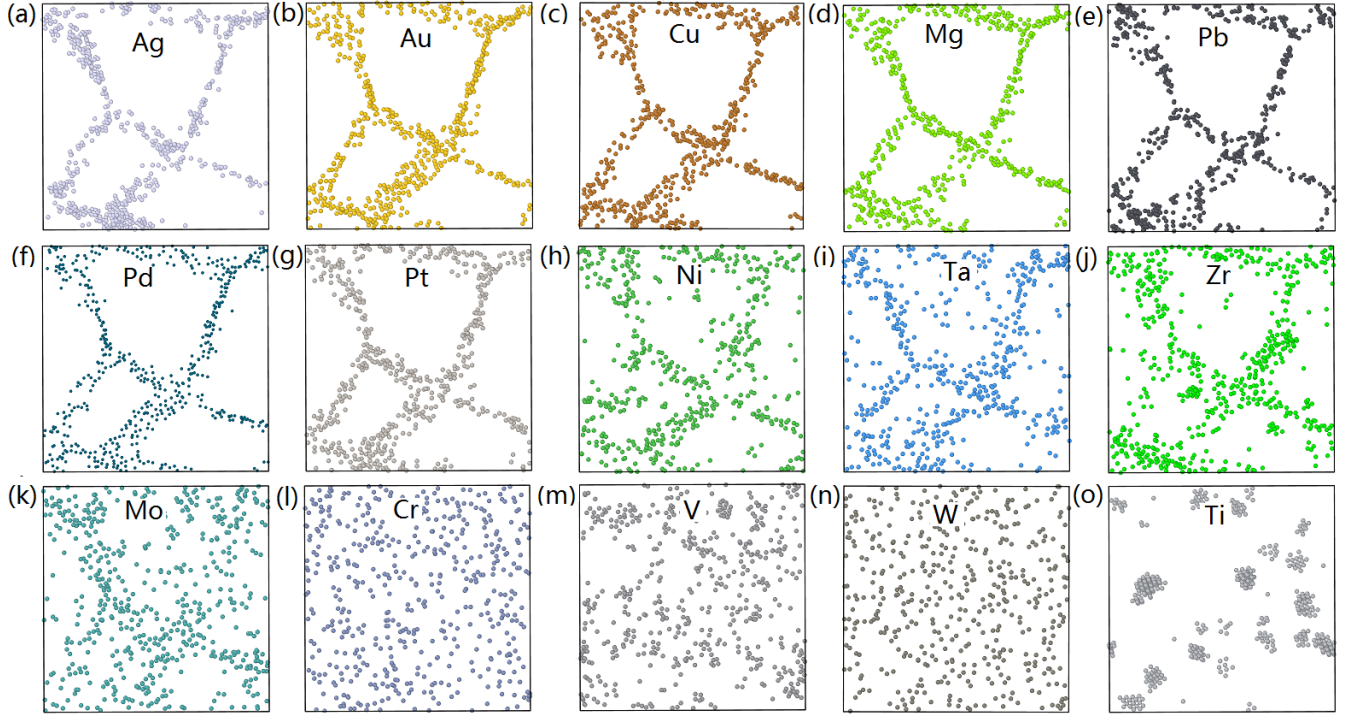


FIG. 3. Distribution of solute atoms in the 2-nm-thick slices (xy plane, z-axis range 10 to 12 nm) extracted from the equilibrated structures obtained from MCMD simulations. (a-g) for Ag, Au, Cu, Mg, Pb, Pd, Pt (Category 1: Fully segregated to GBs); (h-k) for Ni, Ta, Zr, Mo (Category 2: Partially segregated to GBs); (l-n) for Cr, V, W (Category 3: Random distribution); and (o) for Ti (Category 4: Precipitation within the grains).

fracture.

To further investigate the impact of solute segregation on the strength of polycrystalline Al, Pt and Pb were selected due to their significant influence on its strength. However, the influence of Mg solute remains contentious in DFT studies, with conflicting findings on whether Mg strengthens or embrittles GBs^{36,38,48,49}. Nevertheless, our analysis in Fig 4 reveals that Mg indeed embrittles polycrystalline Al, consistent with experimental observations⁵⁰. In Fig 6, snapshots of Mg, Pt and Pb solute segregation in polycrystalline Al under different strains are presented.

In Fig 6(a), we observe that the strain (5.3%) for Shockley dislocation nucleation is greater than that of pure polycrystalline Al (4.9%), as illustrated in Fig 5. This can be attributed to the hindrance of dislocation nucleation and movement by Mg segregation at the GB due to its large size. As shown in Fig 4 (b), the stress of Mg is greater than that of pure Al in the same strain (range 0-5.3%); however, once dislocations are emitted, the stress curves overlap in the strain range of 5.3-7.5%. Moreover, Mg may reduce the charge density at the GBs³⁹, and Mg-Al bond weakens the GB cohesion, leading to premature cracking of the GBs.

Unlike Mg, Pb promotes the formation of Shockley dislocation, as shown in Fig 6(i). In MCMD simulations, Pd atoms segregate from the bulk to the GB, leading to a

decrease in the system's energy. Due to the significantly larger size of Pb compared to Al, the segregation of Pb at the loose positions of the GB still causes expansion of both the GB and the system, increasing local stress at the GB. Consequently, this lowers the cohesion at the GB and provides a driving force for the nucleation of dislocations. This size effect was also discussed at Ni and Ag GB⁵¹, consistent with our findings. In addition, Pb is also a well-known embrittling element⁹, which significantly reduces the cohesion of GBs and further promotes the nucleation of cracks at GBs, as depicted in Fig 6(k).

In contrast, Pt acts as a strengthening solute⁹. When Pt segregates at Al GBs, it increases the cohesion of GB, thereby raising the stress required for dislocation nucleation and emission from the GBs, as illustrated in Fig 6(e). When the stress for crack nucleation at the GBs exceeds the stress for dislocation and stacking fault nucleation and emission from the GB, dislocation nucleation and movement occur prior to crack formation during the tensile process. As depicted in Fig 6(f), before crack nucleation, the movement and transformation of Shockley dislocations ($1/6\langle 112 \rangle$ Shockley to $1/6\langle 110 \rangle$ stair-rod dislocation) are observed in the crack area. The formation of the stair-rod dislocation marks the onset of plastic instability and indicates that cracks or holes will form^{47,52}.

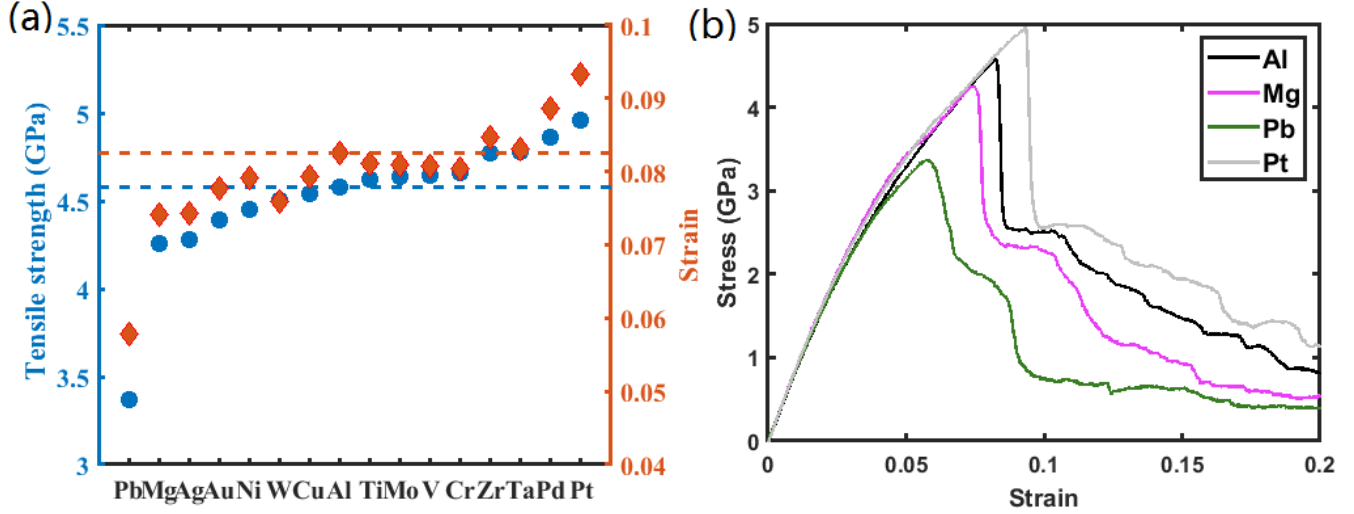


FIG. 4. (a) Tensile strength as a function of solutes. Blue spheres represent the tensile strength of the polycrystalline binary systems, displayed on the left Y-axis, while red diamonds represent the corresponding strain at the tensile strength of the polycrystalline system, indicated on the right Y-axis. Blue dashed line and red dashed line correspond to values of pure polycrystalline Al, respectively. (b) The stress-strain curves for Al, Mg, Pb, and Pt.

IV. SUMMARY AND CONCLUSIONS

In conclusion, we have successfully implemented a canonical-ensemble MCMD algorithm in GPUMD, demonstrating its accuracy and unprecedented efficiency. Leveraging this efficient MCMD algorithm, we investigated the segregation behavior of 15 solutes in polycrystalline Al employing a general-purpose unified UNEP-v1 machine-learned potential for 16 elemental metals and their alloys²³. Our findings reveal distinct segregation patterns, with Ag, Au, Cu, Mg, Pb, Pd, Pt fully segregated at GBs, while Ni, Ta, Mo and Zr partially segregated at GBs. Notably, Cr, V, W and Ti do not segregate at the GBs, with Ti precipitating in the form of a BCC TiAl structure within the crystals.

Furthermore, uniaxial tensile tests on 15 binary polycrystalline Al alloys demonstrate a significant reinforcement effect by Pt and Pd, whereas Pb induces substantial embrittlement. Through the analysis of microstructure, dislocation nucleation, and crack nucleation, it was found that during the deformation process of polycrystalline Al, GBs play a pivotal role in determining its mechanical properties, and solute segregation significantly impacts the GBs structure and cohesion, thereby affecting dislocation and crack nucleation, ultimately leading to strengthening or embrittlement of polycrystalline Al.

Our efficient MCMD approach, coupled with unified neuroevolution potential in GPUMD, not only furnishes valuable tools for accurately and efficiently simulating solute segregation and chemical ordering in alloy systems, but also offers insights for future simulations and theoretical guidance for the design of polycrystalline alloy materials. We expect that our developed methods will also

prove valuable for investigating a wide range of multi-component materials, including medium-entropy materials, high-entropy materials, and complex concentrated alloys.

V. ACKNOWLEDGMENTS

We acknowledge support from the National Natural Science Foundation of China (NSFC) (No. 52071020).

Data availability:

The UNEP-v1 model is freely available at the Zenodo repository with following link: <https://doi.org/10.5281/zenodo.10081677>. The source code and documentation for GPUMD are available at <https://github.com/brucefan1983/GPUMD> and <https://gpumd.org>, respectively.

Declaration of competing interest:

The authors declare that they have no competing interests.

Appendix A: Input parameters for MCMD simulations in GPUMD

MCMD simulations with NEP models can be conducted using the `gpumd` executable in the GPUMD package²⁸. The parameters controlling the simulations are specified in the `run.in` input file. Below is an example of the contents of the `run.in` input file for one system. The keyword `mc` invokes the MC trials during

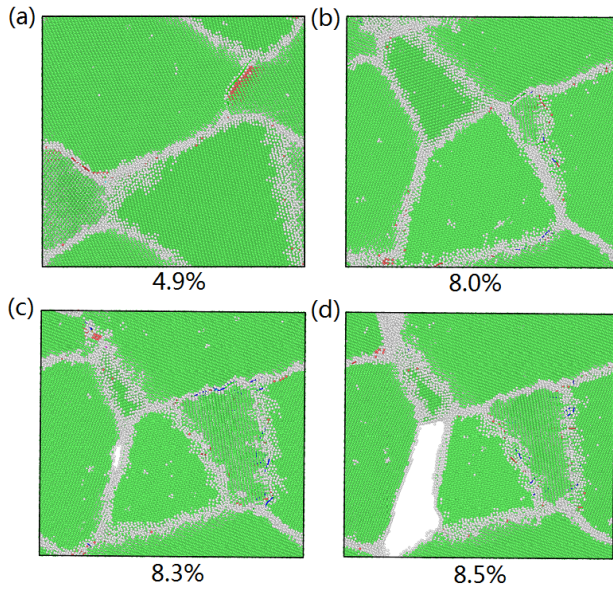


FIG. 5. Snapshots of 2-nm-thick slices for pure polycrystalline Al under different strains: (a) 4.9% (yz plane, x-axis range 0.8 to 2.8 nm), (b) 8.0% (xy plane, z-axis range 11 to 13 nm), (c) 8.3% (xy plane, z-axis range 11 to 13 nm), and (d) 8.5% (xy plane, z-axis range 11 to 13 nm). Green spheres represent FCC atoms, red spheres represent HCP atoms, and blue line represents $1/6\langle 112 \rangle$ Shockley dislocation, purple line represents $1/6\langle 110 \rangle$ stair-rod dislocation. Gray spheres represent atoms at the GBs.

the MD simulation. The parameter `canonical` indicates that the MC ensemble is canonical, conserving the number of atoms for each species. The parameters 100 100 mean performing 100 MC trials after every 100 MD steps. The parameters 300 300 denote maintaining the temperature in the MC trials at 300 K.

```
# setup
potential nep.txt
velocity 300

# MCMD simulation
ensemble      npt_mttk temp 300 300 iso 0 0
time_step     1
mc            canonical 100 100 300 300
dump_thermo   100
dump_exyz     50000
dump_restart  10000
run           5000000
```

Appendix B: Inputs for tensile loading simulations in GPUMD

Tensile loading simulations with NEP models can also be performed using the `gpumd` executable in the GPUMD package²⁸. The relevant contents of the `run.in` input file are provided below. Tensile loading is initiated by

the keyword `deform`, with a deformation speed of 2×10^{-5} Å/fs, corresponding to an engineering strain rate of 10^8 s⁻¹ for a system with a linear size of 200 Å. Due to an implementation restriction in GPUMD, the `deform` keyword can only be effective by using an NpT ensemble. Therefore, we used a very large relaxation time for the barostat to effectively convert the NpT ensemble into the NVT ensemble intended for use.

```
# tensile loading simulation
ensemble      npt_scr 300 300 100
              0 0 0 100 100 100 1e10
time_step     1
deform        0.00002 0 1 0
dump_thermo   100
dump_exyz     1000
dump_restart  10000
run           3000000
```

REFERENCES

- ¹P. Schloth, A. Menzel, J. Fife, J. Wagner, H. Van Swygenhoven, and J.-M. Drezet, “Early cluster formation during rapid cooling of an Al-Cu-Mg alloy: In situ small-angle x-ray scattering,” *Scripta Materialia* **108**, 56–59 (2015).
- ²S. Wang and M. Starink, “Two types of s phase precipitates in Al-Cu-Mg alloys,” *Acta Materialia* **55**, 933–941 (2007).
- ³A. D. Rollett, G. Gottstein, L. S. Shvindlerman, and D. A. Molodov, “Grain boundary mobility - a brief review,” *International Journal of Materials Research* **95**, 226–229 (2004).
- ⁴H. C. Rogers, “Hydrogen embrittlement of metals,” *Science* **159**, 1057–1064 (1968).
- ⁵A. King, G. Johnson, D. Engelberg, W. Ludwig, and J. Marrow, “Observations of intergranular stress corrosion cracking in a grain-mapped polycrystal,” *Science* **321**, 382–385 (2008).
- ⁶D. Raabe, M. Herbig, S. Sandlöbes, Y. Li, D. Tytko, M. Kuzmina, D. Ponge, and P.-P. Choi, “Grain boundary segregation engineering in metallic alloys: A pathway to the design of interfaces,” *Current Opinion in Solid State and Materials Science* **18**, 253–261 (2014).
- ⁷D. Raabe, S. Sandlöbes, J. Millán, D. Ponge, H. Assadi, M. Herbig, and P.-P. Choi, “Segregation engineering enables nanoscale martensite to austenite phase transformation at grain boundaries: A pathway to ductile martensite,” *Acta Materialia* **61**, 6132–6152 (2013).
- ⁸Z. Yu, P. R. Cantwell, Q. Gao, D. Yin, Y. Zhang, N. Zhou, G. S. Rohrer, M. Widom, J. Luo, and M. P. Harmer, “Segregation-induced ordered superstructures at general grain boundaries in a nickel-bismuth alloy,” *Science* **358**, 97–101 (2017).
- ⁹P. Lejček, M. Šob, and V. Paidar, “Interfacial segregation and grain boundary embrittlement: An overview and critical assessment of experimental data and calcu-

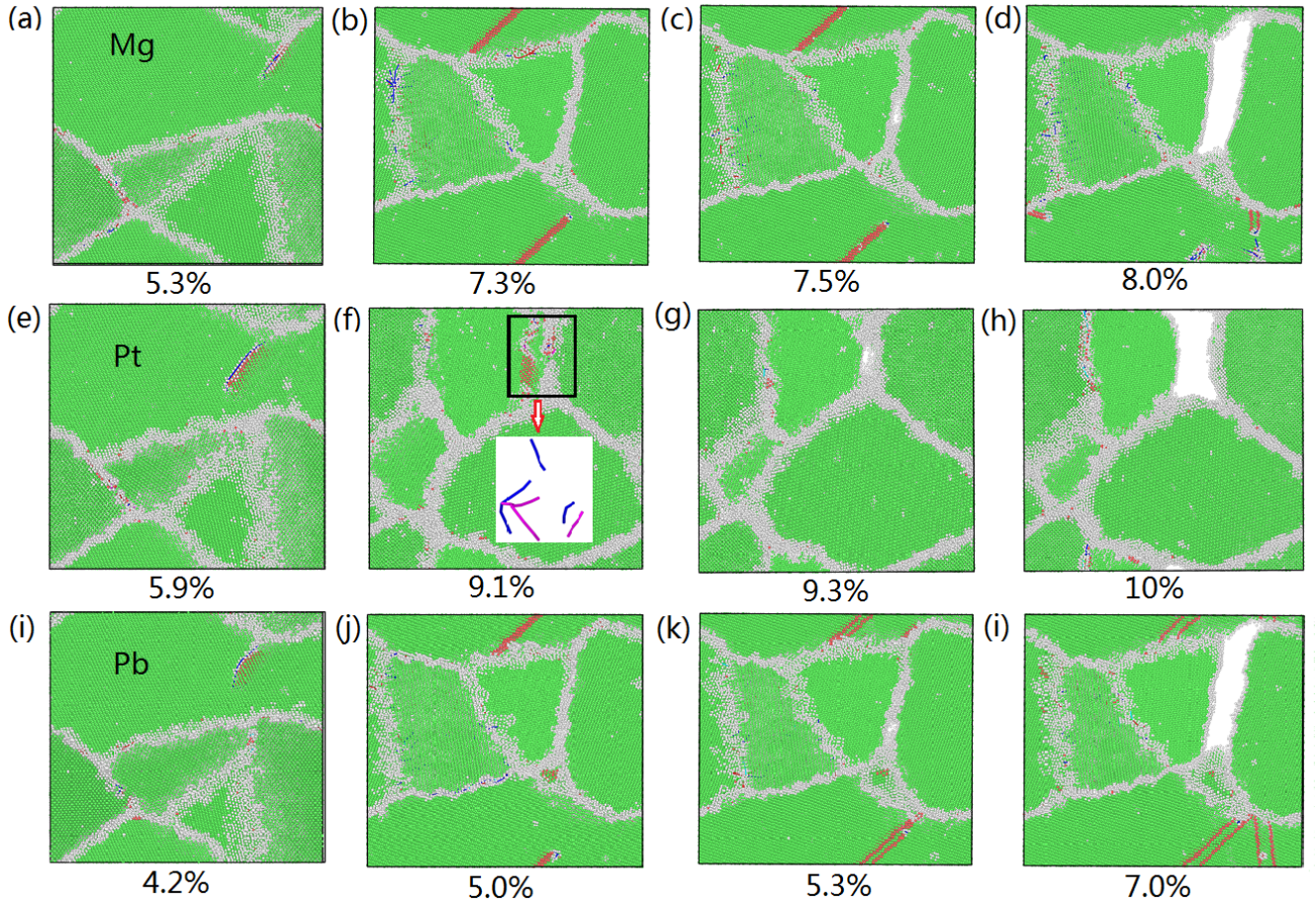


FIG. 6. Snapshots of 2-nm-thick slices for polycrystalline binary systems under different strains: (a-d) Mg, 5.3% strain (yz plane, x-axis range 2 to 4 nm), the remaining strains (xy plane, z-axis range 12 to 14 nm); (e-h) Pt, 5.9% strain (yz plane, x-axis range 0.3 to 2.3 nm), the remaining strains (xy plane, z-axis range 4 to 6 nm); (i-l) Pb, 4.2% strain (yz plane, x-axis range 2 to 4 nm), the remaining strains (xy plane, z-axis range 12 to 14 nm). Green spheres represent FCC atoms, red spheres represent HCP atoms, blue lines represent $1/6\langle 112 \rangle$ Shockley dislocations. In panel (f) inset, purple lines represent $1/6\langle 110 \rangle$ stair-rod dislocation. Pt segregation markedly enhances the cohesion of GBs, with dislocation nucleation and transformation occurring earlier than crack nucleation, to accommodate the redistribution of stress during the deformation. The embrittling element does not exhibit this phenomenon.

- lated results,” *Progress in Materials Science* **87**, 83–139 (2017).
- ¹⁰R. Mahjoub, K. J. Laws, N. Stanford, and M. Ferry, “General trends between solute segregation tendency and grain boundary character in aluminum - an ab initio study,” *Acta Materialia* **158**, 257–268 (2018).
- ¹¹X. Wu, Y.-W. You, X.-S. Kong, J.-L. Chen, G.-N. Luo, G.-H. Lu, C. Liu, and Z. Wang, “First-principles determination of grain boundary strengthening in tungsten: Dependence on grain boundary structure and metallic radius of solute,” *Acta Materialia* **120**, 315–326 (2016).
- ¹²V. Razumovskiy, A. Lozovoi, and I. Razumovskii, “First-principles-aided design of a new Ni-base superalloy: Influence of transition metal alloying elements on grain boundary and bulk cohesion,” *Acta Materialia* **82**, 369–377 (2015).
- ¹³H. A. Murdoch and C. A. Schuh, “Estimation of grain boundary segregation enthalpy and its role in stable nanocrystalline alloy design,” *Journal of Materials Research* **28**, 2154–2163 (2013).
- ¹⁴T. Liu, B. Zhang, H. Yin, X. He, M. Liu, J. Qiu, and W. Liu, “First-principles study on the corrosion resistance of iron oxide surface and grain boundary in austenitic steel to lead–bismuth eutectic,” *Applied Surface Science* **640**, 158409 (2023).
- ¹⁵W. Wan, C. Tang, and W. Zou, “Exploring silicon [001] small angle symmetric tilt grain boundaries: Structures, energies and stress fields,” *Applied Surface Science* **599**, 153828 (2022).
- ¹⁶K. Song, S. Cao, Y. Bao, P. Qian, and Y. Su, “Designing hydrogen embrittlement-resistant grain boundary in steel by alloying elements segregation: First-principles calculations,” *Applied Surface Science* **656**, 159684 (2024).

- ¹⁷M. Papanikolaou and K. Salonitis, “Grain size effects on nanocutting behaviour modelling based on molecular dynamics simulations,” *Applied Surface Science* **540**, 148291 (2021).
- ¹⁸L. Yuan, P. Jing, D. Shan, and B. Guo, “The effect of inclination angle on the plastic deformation behavior of bicrystalline silver nanowires with 3 asymmetric tilt grain boundaries,” *Applied Surface Science* **392**, 1153–1164 (2017).
- ¹⁹W. Huang, J. Tang, W. Zhou, J. Wen, and M. Yi, “Molecular dynamics simulations of ultrasonic vibration-assisted grinding of polycrystalline iron: Nanoscale plastic deformation mechanism and microstructural evolution,” *Applied Surface Science* **640**, 158440 (2023).
- ²⁰R. Koju and Y. Mishin, “Atomistic study of grain-boundary segregation and grain-boundary diffusion in Al-Mg alloys,” *Acta Materialia* **201**, 596–603 (2020).
- ²¹M. S. Daw and M. I. Baskes, “Embedded-atom method: Derivation and application to impurities, surfaces, and other defects in metals,” *Phys. Rev. B* **29**, 6443–6453 (1984).
- ²²M. W. Finnis and J. E. Sinclair, “A simple empirical n-body potential for transition metals,” *Philosophical Magazine A* **50**, 45–55 (1984).
- ²³K. Song, R. Zhao, J. Liu, Y. Wang, E. Lindgren, Y. Wang, S. Chen, K. Xu, T. Liang, P. Ying, N. Xu, Z. Zhao, J. Shi, J. Wang, S. Lyu, Z. Zeng, S. Liang, H. Dong, L. Sun, Y. Chen, Z. Zhang, W. Guo, P. Qian, J. Sun, P. Erhart, T. Ala-Nissila, Y. Su, and Z. Fan, “General-purpose machine-learned potential for 16 elemental metals and their alloys,” (2023), [arXiv:2311.04732 \[cond-mat.mtrl-sci\]](https://arxiv.org/abs/2311.04732).
- ²⁴Z. Fan, Z. Zeng, C. Zhang, Y. Wang, K. Song, H. Dong, Y. Chen, and T. Ala-Nissila, “Neuroevolution machine learning potentials: Combining high accuracy and low cost in atomistic simulations and application to heat transport,” *Phys. Rev. B* **104**, 104309 (2021).
- ²⁵Z. Fan, “Improving the accuracy of the neuroevolution machine learning potential for multi-component systems,” *Journal of Physics: Condensed Matter* **34**, 125902 (2022).
- ²⁶Z. Fan, Y. Wang, P. Ying, K. Song, J. Wang, Y. Wang, Z. Zeng, K. Xu, E. Lindgren, J. M. Rahm, A. J. Gabourie, J. Liu, H. Dong, J. Wu, Y. Chen, Z. Zhong, J. Sun, P. Erhart, Y. Su, and T. Ala-Nissila, “Gpumd: A package for constructing accurate machine-learned potentials and performing highly efficient atomistic simulations,” *The Journal of Chemical Physics* **157**, 114801 (2022).
- ²⁷X. W. Zhou, R. A. Johnson, and H. N. G. Wadley, “Misfit-energy-increasing dislocations in vapor-deposited CoFe/NiFe multilayers,” *Phys. Rev. B* **69**, 144113 (2004).
- ²⁸Z. Fan, W. Chen, V. Vierimaa, and A. Harju, “Efficient molecular dynamics simulations with many-body potentials on graphics processing units,” *Computer Physics Communications* **218**, 10 – 16 (2017).
- ²⁹P. Hirel, “Atomsk: A tool for manipulating and converting atomic data files,” *Computer Physics Communications* **197**, 212–219 (2015).
- ³⁰A. P. Thompson, H. M. Aktulga, R. Berger, D. S. Bolintineanu, W. M. Brown, P. S. Crozier, P. J. in ’t Veld, A. Kohlmeyer, S. G. Moore, T. D. Nguyen, R. Shan, M. J. Stevens, J. Tranchida, C. Trott, and S. J. Plimpton, “LAMMPS - a flexible simulation tool for particle-based materials modeling at the atomic, meso, and continuum scales,” *Computer Physics Communications* **271**, 108171 (2022).
- ³¹A. Stukowski, “Visualization and analysis of atomistic simulation data with ovito—the open visualization tool,” *Modelling and Simulation in Materials Science and Engineering* **18**, 015012 (2009).
- ³²J. Pickens and T. Langan, “The effect of solution heat-treatment on grain boundary segregation and stress-corrosion cracking of Al-Zn-Mg alloys,” *Metallurgical Transactions A* **18**, 1735–1744 (1987).
- ³³R. Jones, D. Baer, M. Danielson, and J. Vetrano, “Role of mg in the stress corrosion cracking of an Al-Mg alloy,” *Metallurgical and Materials Transactions A* **32**, 1699–1711 (2001).
- ³⁴T. Malis and M. Chaturvedi, “Grain-boundary segregation in an al-8 wt% mg alloy,” *Journal of Materials Science* **17**, 1479–1486 (1982).
- ³⁵G. Sha, L. Yao, X. Liao, S. P. Ringer, Z. Chao Duan, and T. G. Langdon, “Segregation of solute elements at grain boundaries in an ultrafine grained Al-Zn-Mg-Cu alloy,” *Ultramicroscopy* **111**, 500–505 (2011).
- ³⁶X.-Y. Liu and J. Adams, “Grain-boundary segregation in Al-10%Mg alloys at hot working temperatures,” *Acta Materialia* **46**, 3467–3476 (1998).
- ³⁷X. Liu, X. Wang, J. Wang, and H. Zhang, “First-principles investigation of mg segregation at 11(113) grain boundaries in al,” *Journal of Physics: Condensed Matter* **17**, 4301 (2005).
- ³⁸S. Zhang, O. Y. Kontsevoi, A. J. Freeman, and G. B. Olson, “Cohesion enhancing effect of magnesium in aluminum grain boundary: A first-principles determination,” *Applied Physics Letters* **100**, 231904 (2012).
- ³⁹D. Zhao, O. M. Løvvik, K. Marthinsen, and Y. Li, “Segregation of Mg, Cu and their effects on the strength of al 5 (210)[001] symmetrical tilt grain boundary,” *Acta Materialia* **145**, 235–246 (2018).
- ⁴⁰L. Karkina, I. Karkin, A. Kuznetsov, I. Razumov, P. Korzhavyi, and Y. Gornostyrev, “Solute-grain boundary interaction and segregation formation in Al: First principles calculations and molecular dynamics modeling,” *Computational Materials Science* **112**, 18–26 (2016).
- ⁴¹H. Clemens and S. Mayer, “Design, processing, microstructure, properties, and applications of advanced intermetallic TiAl alloys,” *Advanced Engineering Materials* **15**, 191–215 (2013).
- ⁴²O. Genc and R. Unal, “Development of gamma titanium aluminide alloys: A review,” *Journal of Alloys and Compounds* **929**, 167262 (2022).

- ⁴³X. Wu, “Review of alloy and process development of TiAl alloys,” *Intermetallics* **14**, 1114–1122 (2006).
- ⁴⁴X. L. Wu and Y. T. Zhu, “Partial-dislocation-mediated processes in nanocrystalline Ni with nonequilibrium grain boundaries,” *Applied Physics Letters* **89**, 031922 (2006).
- ⁴⁵H. Van Swygenhoven, P. M. Derlet, and A. Hasnaoui, “Atomic mechanism for dislocation emission from nanosized grain boundaries,” *Phys. Rev. B* **66**, 024101 (2002).
- ⁴⁶L. Zhang, C. Lu, K. Tieu, L. Pei, X. Zhao, and K. Cheng, “Molecular dynamics study on the grain boundary dislocation source in nanocrystalline copper under tensile loading,” *Materials Research Express* **2**, 035009 (2015).
- ⁴⁷Y. Cui, K. Song, Y. Bao, Y. Zhu, Q. Liu, and P. Qian, “Effect of Cu and Mg co-segregation on the strength of the Al grain boundaries: A molecular dynamics simulation,” *Computational Materials Science* **229**, 112391 (2023).
- ⁴⁸R. Song, M. Tseng, B. Zhang, J. Liu, Z. Jin, and K. Shin, “Grain boundary segregation and hydrogen-induced fracture in 7050 aluminium alloy,” *Acta Materialia* **44**, 3241–3248 (1996).
- ⁴⁹V. I. Razumovskiy, A. Ruban, I. Razumovskii, A. Lozovoi, V. Butrim, and Y. Vekilov, “The effect of alloying elements on grain boundary and bulk cohesion in aluminum alloys: An ab initio study,” *Scripta Materialia* **65**, 926–929 (2011).
- ⁵⁰S. H. Na, M. S. Yang, and S. W. Nam, “Effects of stress amplitude and internal stress on the grain boundary deformation behavior under high temperature creep in an Al2.9%Mg alloy,” *Scripta Metallurgica et Materialia* **32**, 627–632 (1995).
- ⁵¹B. Lezzar, O. Khalfallah, A. Larere, V. Paidar, and O. Hardouin Duparc, “Detailed analysis of the segregation driving forces for Ni(Ag) and Ag(Ni) in the $\sigma = 11\ 113$ and $11\ 332$ grain boundaries,” *Acta Materialia* **52**, 2809–2818 (2004).
- ⁵²S. Ma, J. Zhang, B. Xu, Y. Xiong, W. Shao, and S. Zhao, “Chemical short-range ordering regulated dislocation cross slip in high-entropy alloys,” *Journal of Alloys and Compounds* **911**, 165144 (2022).